Dynamic effects in a clearance-sealed piston prover for gas flow measurements

2011 Metrologia 48 123

(http://iopscience.iop.org/0026-1394/48/3/006)

Metrologia **48** (2011) 123–132 doi:10.1088/0026-1394/48/3/006

Dynamic effects in a clearance-sealed piston prover for gas flow measurements

Jože Kutin, Gregor Bobovnik and Ivan Bajsić

Laboratory of Measurements in Process Engineering, Faculty of Mechanical Engineering, University of Ljubljana, Aškerčeva 6, SI-1000 Ljubljana, Slovenia

E-mail: joze.kutin@fs.uni-lj.si

Received 25 October 2010, in final form 20 January 2011
Published 1 March 2011
Online at stacks.iop.org/Met/48/123

Abstract

A piston prover determines the gas flow rate by measuring the time interval that a movable piston inside a cylinder needs to pass a known volume of gas at a defined pressure and temperature. This paper deals with the dynamic effects related to the operation of a high-speed, clearance-sealed realization of the piston prover concept. Its dynamic characteristics are analysed by means of pressure-response measurements and lumped-element mathematical modelling. The experimental results show that the pressure oscillations during the timing cycle increase significantly above a certain flow rate and have multiple frequency components. They could be related to the resonance effects of the piston oscillator, which is excited by the flow instabilities of the gas flowing in the cylinder below the piston. The simulations show that the sensitivity to the dynamic pressure effects depends on the properties of the thermodynamic gas processes being adiabatic, polytropic or isothermal. A new, modified flow equation of the piston prover, which considers the polytropic index as an input variable, is proposed.

(Some figures in this article are in colour only in the electronic version)

1. Introduction

The piston prover represents a common gas flow primary standard [1–5]. Its principle of operation is based on determining the time interval that a piston needs to pass a known volume of gas at a defined pressure and temperature. Based on the law of the conservation of mass for the measured time interval $\Delta t = t_2 - t_1$ of the piston prover, the average inlet mass flow rate can be defined as [1]

$$q_m = \frac{\rho_{m,2} V_m}{\Delta t} + \frac{\left(\rho_{d,2} - \rho_{d,1}\right) V_d}{\Delta t} + q_{m,l}, \qquad (1)$$

where V_m is the volume of gas collected by the piston prover during the interval Δt (measuring volume), $\rho_{m,2}$ is the mean density of the gas in V_m at time t_2, V_d is the connecting volume of the gas between the selected inlet transfer point and the piston at time t_1 (dead volume), $(\rho_{d,2} - \rho_{d,1})$ is the change in the mean density of the gas in V_d during the interval Δt and $q_{m,l}$ is the leakage flow. The first term on the right-hand side of equation (1) represents the uncorrected, measured mass flow rate. The second and third terms correct for the storage and the leakage effects, respectively.

Figure 1 shows a schematic of the flow cell of a commercially available, high-speed, clearance-sealed piston prover [6–8] that was used in the experimental work described in this paper. It operates by collecting the gas below the piston, which causes the piston to move upwards. The piston is made of graphite and the cylinder is made of borosilicate glass. The piston and the cylinder are closely fitted with a clearance of the order of 10 µm. The infrared light emitters and sensors are used to detect the passage of the piston. The flow cell also contains the integrated temperature and (fast-response) gauge pressure sensors positioned at the entrance to the cylinder. The base holds the computer, the time base and the barometric pressure sensor. This instrument's standard volume flow rate reading is calculated as follows:

$$q_s = \frac{q_m}{\rho_s} = \frac{V_m}{\Delta t}\left(\frac{p_2}{p_s} + \frac{p_2 - p_1}{p_s}\frac{V_d}{V_m}\right)\frac{T_s}{T} + q_{s,l}, \qquad (2)$$

where ρ_s is the standard density of the gas under the defined standard conditions p_s and T_s, p_1 and p_2 are the absolute gas pressures at times t_1 and t_2, respectively, T is the gas temperature and $q_{s,l}$ is the leakage flow through the piston/cylinder clearance.

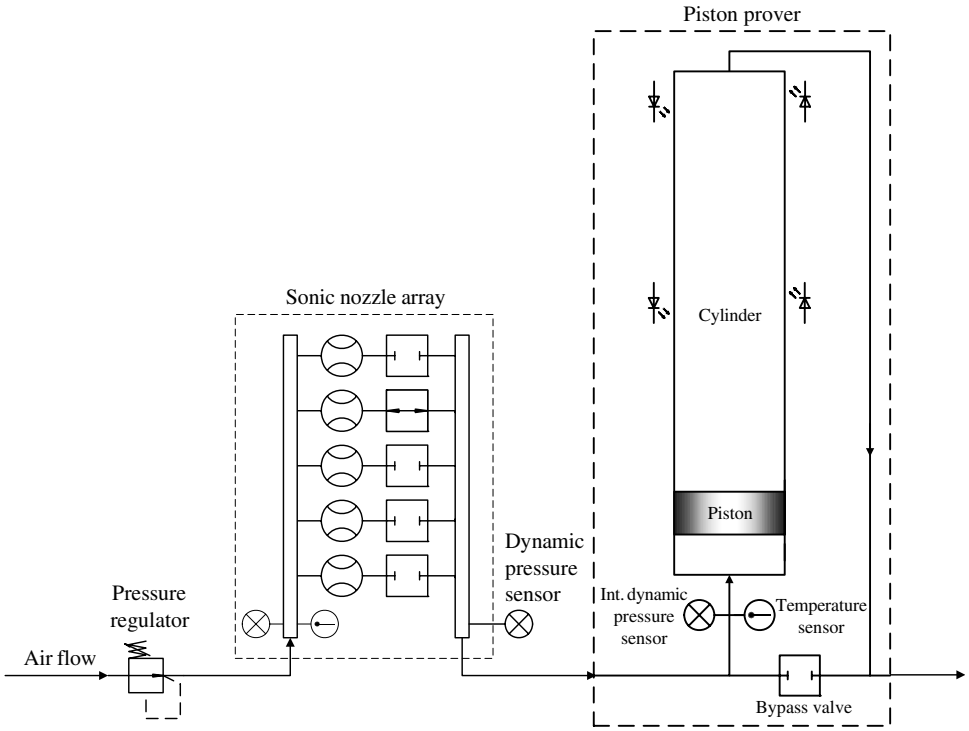

Figure 1. Scheme of the measurement system with the piston prover.

The clearance leakage flow is treated as a laminar Couette–Poiseuille flow. The Poiseuille flow component, which is driven by a pressure difference on the piston, is estimated by the instrument's leakage self-test. During this leakage self-test, the outlet port is closed, the flow cell is inverted and the time of the piston's descent is measured. The result for the Poiseuille leakage flow rate is subsequently employed in the Poiseuille law to estimate the clearance thickness δ. The Couette flow component, which is driven by the relative motion between the piston and the cylinder, is considered as the reduced effective diameter of the cylinder from $D + 2\delta$ to $D + \delta$, where D represents the measured piston diameter (more details can be found in [6, 7]).

The flow equation (2) can be derived from equation (1), if one considers $\rho = p/(ZRT)$, where Z is the gas compressibility and R is the gas constant, and further assumes that the gas temperature is constant, the gas pressure distribution is spatially homogeneous and the gas compressibility changes are negligible. In [7] it was proposed that some linear combination of the inlet gas temperature during the measurement and the ejected gas temperature after the measurement could be used to take into account possible temperature variations.

One of the important features of this piston prover is its high-speed operation. As an illustration, the smallest Δt collection time interval (corresponding to the maximum flow rate) in the flow cell employed in this paper is about 0.15 s. As discussed in [6, 7], the piston prover is potentially subjected to 'accelerative, oscillatory and piston-jamming effects', which result in rapid changes in the gas pressure. For this reason, the fast-response gauge pressure sensor is built into the flow cell to measure the dynamic pressures and perform corrections to the dynamic error [8].

The research work presented in this paper is fully focused on the dynamic pressure effects in piston provers for gas flow measurements. The methods of investigation combine an experimental analysis of the previously described clearance-sealed piston prover and a theoretical analysis using the lumped-element mathematical model. There are two main contributions of this paper. The first contribution is represented by the study of the dynamic pressure conditions that arise during the operation of the piston prover. The experimentally identified amplitudes and frequency characteristics of the pressure variations indicate some possible mechanisms of their excitation and amplification. The second contribution is represented by a study of the effects of the dynamic pressure conditions on the piston prover's flow rate reading. The thermodynamic nature of the gas processes (being adiabatic, polytropic or isothermal) is identified as an influencing parameter on the device's measuring characteristics. We propose a new, modified flow equation for the piston prover, which is found, on the basis of its validation using the mathematical model in section 5, to be more suitable for a compensation of non-isothermal dynamic pressure variations than the flow equation currently used in the respective piston prover.

This paper is organized as follows. Section 2 describes the dynamic mathematical model of the piston prover, which is later employed for the interpretation of the dynamic pressure responses and for the validation of the piston prover's flow equations. Section 3 describes the experimental set-up for the measurements with the clearance-sealed piston prover. Section 4 presents the experimental results of the pressure variations during the piston prover's operation and their detailed analysis. Section 5 deals with the theoretical

error analysis of the different forms of the piston prover's flow equations under dynamic conditions, including the newly derived polytropic flow equation. Section 6 presents a discussion of the experimental results relating to the repeatability of the clearance-sealed piston prover. The conclusions and open questions are summarized in section 7.

2. Dynamic mathematical model of the piston prover

The dynamic mathematical model of the piston prover in this paper is based on lumped-element models, which can be found, for instance, being applied in studies of the dynamics of pneumatic cylinders [9, 10] and free-piston Stirling engines [11, 12]. The main modelling assumptions are as follows.

The piston is modelled as a solid body with one degree of freedom that is defined by its position x in an upward direction along the cylinder. The dynamic equation of the piston's motion can be expressed as the balance of the inertial force, the damping force, the resulting pressure force and the gravitational force:

$$m\ddot{x} = -c\dot{x} - mg + A\,(p - P_{\mathrm{a}})\,, \tag{3}$$

where $\dot{x}$ is the piston's velocity, $\ddot{x}$ is the piston's acceleration, m is the piston's mass, c is the damping coefficient, g is the gravitational acceleration, $A = \pi D^2/4$ is the piston's cross-sectional area and $(p - P_{\mathrm{a}})$ is the pressure difference between the inlet and the outlet sides of the piston. The outlet pressure is assumed to remain constant and be equal to the atmospheric pressure P_{a}.

The model for pressure p in the gas cavity with volume V below the piston will be formulated on the basis of the energy balance by employing the following assumptions. The pressure is considered to be spatially homogeneous, which holds true if the wavelength of the pressure oscillations is large compared with the largest linear dimension of the cavity. The wavelength is defined as c/f, where c is the speed of sound (about 343 m s^{-1} for dry air at 20 °C [13]) and f is the frequency of the pressure oscillation. The thermodynamic process in the gas cavity is considered (for the present) to be adiabatic, which claims no heat exchange with the surroundings or very fast processes with respect to the heat exchange. In addition, the gas is assumed to be ideal and the viscous dissipative effects are neglected. The energy is transported into the gas cavity by means of the mass flow rate $q_{\mathrm{m}} = \rho_{\mathrm{s}} q_{\mathrm{s}}$ and the temperature T, but the potential and kinetic energy terms of the flowing gas are neglected. The energy equation results in a balance of the rate of change of the internal energy, the rate of the work done on the piston and the inlet enthalpy flow rate:

$$\frac{c_v}{R}\left(p\dot{V} + \dot{p}V\right) = -p\dot{V} + c_p T q_{\mathrm{m}}, \tag{4}$$

where c_v is the specific heat at constant volume, c_p is the specific heat at constant pressure and R is the gas constant. Defining the gas volume in terms of the piston position $V = Ax$ and considering $c_p = c_v + R$ and $\gamma = c_p/c_v$, equation (4) gives

$$\dot{p} = \frac{\gamma}{Ax}\left(RTq_{\mathrm{m}} - pA\dot{x}\right). \tag{5}$$

Table 1. Modelling input data.

D	44.5 mm
$\Delta X = X_2 - X_1$	76.2 mm
$X_1/\Delta X$	1.8
$X_0/\Delta X$	0.6
m	24 g
g	9.806 m s^{-2}
c	1 N s m^{-1}
T	295 K
P_{a}	98 kPa

The ratio of the specific heats or adiabatic index γ is about 1.4 for air. The model (5) can be simply transformed into the form valid for an isothermal system by considering $\gamma = 1$. When it is more correct to use an intermediate value, $1 < \gamma < 1.4$, the corresponding processes are called polytropic [13].

The steady-state solution of the mathematical model (3) and (5) can be found in an analytical form. Considering $\ddot{x} = 0$ and $\dot{p} = 0$ gives

$$\dot{X} = \frac{q_{\mathrm{m}}}{\bar{\rho}A} = \frac{q_{\mathrm{m}}}{P/(RT)\,A}, \tag{6}$$

$$P = P_{\mathrm{a}} + \frac{mg + c\dot{X}}{A}, \tag{7}$$

where $\dot{X}$ is the steady-state piston velocity and P is the steady-state gas-cavity pressure.

Furthermore, the system of differential equations (3) and (5) can be solved for the time response of the piston's position $x(t)$, the piston's velocity $\dot{x}(t)$ and the gas-cavity pressure $p(t)$ for some specified initial conditions $x(0) = X_0$, $\dot{x}(0) = \dot{X}_0$ and $p(0) = P_0$. In the simulations within this paper, we considered the initial piston velocity $\dot{X}_0 = 0$ and the cavity pressure $P_0 = P_{\mathrm{a}}$, and the additional condition that the piston cannot be, at any time, at a lower position than the initial value X_0. The system of differential equations was solved using the fourth-order Runge–Kutta fixed-step method ('rkfixed' built-in function) in Mathcad (Mathsoft, Ver. 12.1), with 2×10^5 constant time steps within the piston stroke between X_0 and $1.05X_2$. This means that each time period of the dynamic pressure responses simulated in this paper is represented by more than 3000 time steps. Using the solution for $x(t)$, we further determined the times t_1 and t_2, when the piston passes over the sensing points X_1 and X_2, respectively. The corresponding time interval $\Delta t = t_2 - t_1$ and the pressures p_1 and p_2 were then used to evaluate the measured flow rate with the piston prover.

All the simulations in this paper were performed using the model input data in table 1. Some input data were based on the calibration certificate and the manufacturer's information (D, ΔX, $X_1/\Delta X \equiv V_{\mathrm{d}}/V_{\mathrm{m}}$), whereas others were estimated by the authors, taking into account the environmental conditions and the measurement results.

3. Measurement system

Figure 1 presents a scheme of the measurement system. The working fluid is clean, dry and oil-free compressed air. The

measurement system consists of a pressure regulator, a critical nozzle array (TetraTec, Venturi-shaped critical nozzles) and the piston prover (Sierra Instruments, Cal=Trak SL-800, measuring range 0.5 sL min^{-1} to 50 sL min^{-1}, expanded uncertainty ($k = 2$) 0.15%), which are connected in series. The flow rate was set before each measurement with the help of the pressure regulator and the selected critical nozzle. Critical nozzles operating under sonic conditions represent a stable source of mass flow rate. The flow rate was measured by the piston prover.

In order to measure dynamic pressure variations we used fast-response pressure sensors attached to the flow system at the outlet of the critical nozzle array. The variable-reluctance pressure transmitter (Validyne, P855, measuring range ±1400 Pa, expanded uncertainty ($k = 2$) 0.15% of upper range limit) was used for gauge pressures below 1400 Pa, and the piezoelectric sensor in connection with the charge amplifier (Kistler, 7261&5007, measuring range ±4000 Pa, expanded uncertainty ($k = 2$) 0.25% of upper range limit) for higher pressures. The electrical voltage output signal from the pressure-measurement system was measured with a DAQ board (National Instruments, USB-6251 BNC). The acquisition and processing of the measurement signals, as well as the serial communication with the piston prover, were realized with LabView software (National Instruments, Ver. 8.5). Both pressure-measurement systems had their frequency range limited with a higher order, low-pass filter with a cut-off frequency of 250 Hz.

4. Analysis of dynamic pressure variations

When the piston prover is not active, the inlet gas flows through the bypass valve. However, when the measurement is initiated, the bypass valve is closed and the inlet flow is redirected into a cylinder where it displaces a piston. The piston starts moving and when it reaches its uppermost position, the bypass valve is opened and the piston gradually returns to its initial position. These particular steps are also evident from the measured pressure responses in the inlet gas flow.

Figures 2(*a*) and (*b*) show the measured pressure during the periodic operation of the piston prover for two different gas flow rates of 1.0 sL min^{-1} and 7.5 sL min^{-1}, respectively (the standard conditions are defined at an absolute pressure of 101.325 kPa and a temperature of 20 °C). When the bypass valve is closed, an increase in the mean pressure and an initial pressure overshoot are recorded. For smaller gas flow rates the pressure conditions are more or less constant during the piston stroke, whereas for higher flow rates larger pressure oscillations are visible. Figure 2(*b*) clearly shows that the amplitude variations are similar for consecutive measurement cycles. A further analysis of the pressure responses is presented separately for the initial transient cycle in section 4.1 and for the timing cycle of the piston stroke in section 4.2. The timing length of the piston stroke is approximately equal to the last 45% of the entire piston stroke.

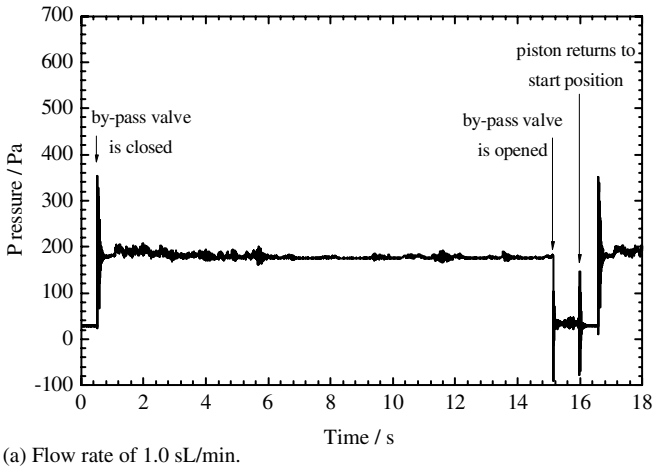

(a) Flow rate of 1.0 sL/min.

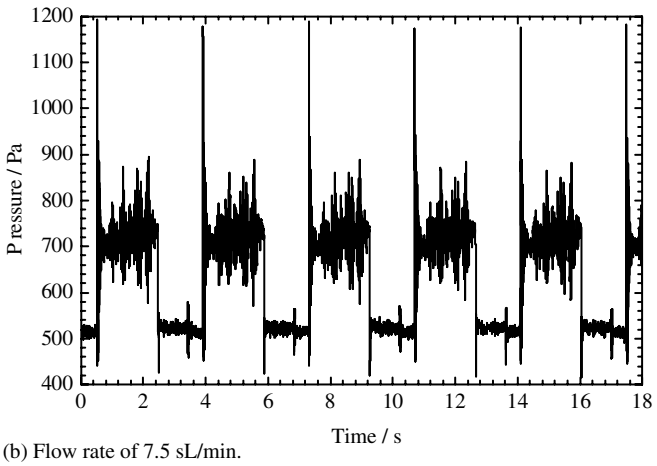

(b) Flow rate of 7.5 sL/min.

Figure 2. Measured time variation of the pressure response during the piston prover's operation for two different flow rates.

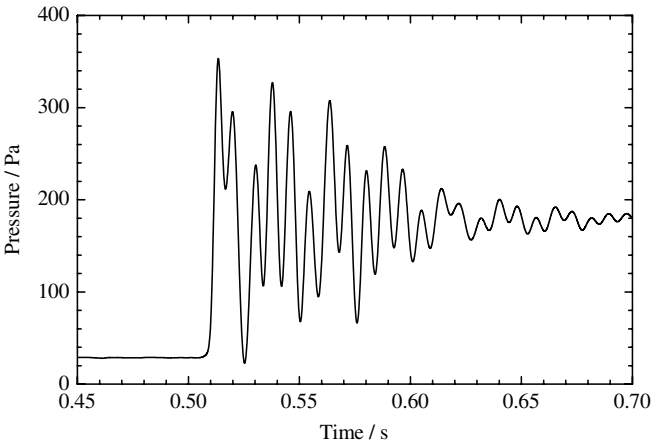

Figure 3. Measured time variation of the initial, transient pressure response (flow rate of 1.0 sL min^{-1}).

4.1. Pressure response during the initial cycle of the piston stroke

The initial, damped pressure oscillation resulting from closing the bypass valve and redirecting the gas flow into the measuring cylinder of the piston prover is shown magnified in figure 3 for the gas flow rate of 1.0 sL min^{-1}. The transient pressure response lasts for approximately 0.15 s and reaches its steady

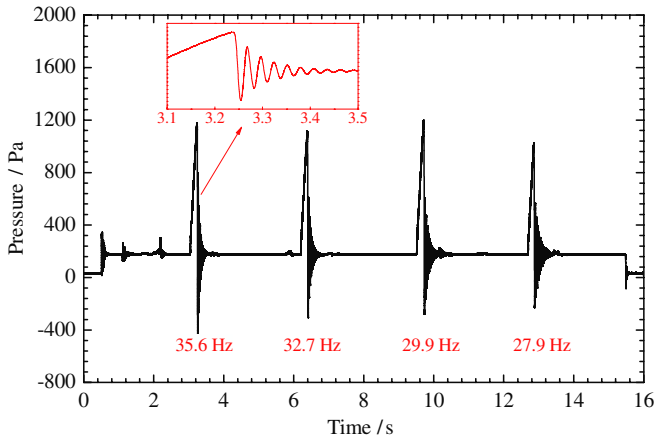

Figure 4. Measured transient pressure response produced by the external disturbances (flow rate of 1.0 sL min^{-1}).

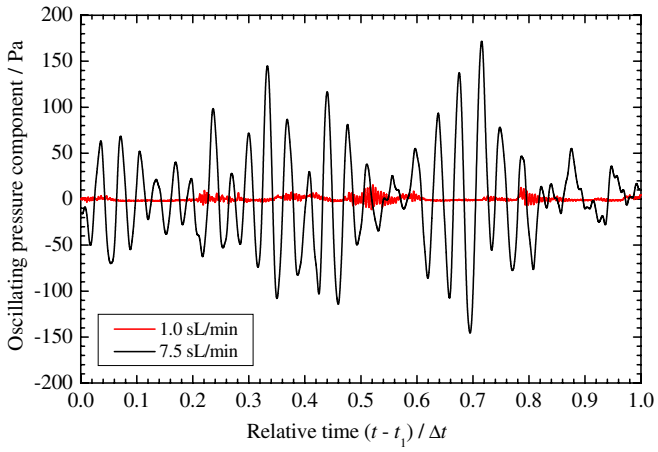

Figure 5. Measured time variation of the oscillating pressure component during the Δt period for two different flow rates.

value, which is about 150 Pa higher than it was before the initiation of the measurement. Such an increase in the average pressure after the initiation of the measurement at the inlet can be related to the pressure difference needed to keep the piston moving with a steady-state velocity upwards in the cylinder. Following equation (7), the gravity and the damping force define the steady-state pressure difference on the piston. In addition, the pressure losses of the gas flow in the piston prover, which are not taken into account in the mathematical model in section 2, also affect the measured pressure response. The initial step change of the average pressure is found to increase with the gas flow rate and is about 600 Pa at 45 sL min^{-1}.

A Fourier frequency analysis of the initial transient pressure response highlights two dominant frequency components at about 39 Hz and 119 Hz. To examine their physical nature, we performed an additional test with external disturbances during the piston stroke, which were made by short time blockages of the outflow. A blockage causes the piston to stop for a short time and induces a natural damped response after the blockage is removed. The resulting damped pressure responses and their characteristic frequencies are shown in figure 4 for four consecutive disturbances. It is evident that the characteristic frequency of 39 Hz in the initial transient decreases continuously during the piston stroke to about 26 Hz at the end, but the frequency of 119 Hz is not seen after the initial transient.

The frequency component of 39 Hz can be related to the natural frequency of the piston oscillator, which represents the piston mass oscillating on the gas spring. The mathematical model in section 2 can be used to model the moving piston oscillator. An approximate expression for the piston's natural frequency can be given as in [13]:

$$f_{\mathrm{p}} = \frac{1}{2\pi}\sqrt{\frac{\gamma P A^2}{mV}}. \tag{8}$$

Because the cavity volume $V = Ax$ increases as the piston moves upwards, the piston's natural frequency decreases during the measuring cycle. Considering the input data from table 1, $\gamma = 1.4$ for the adiabatic system and the steady-state solutions from equations (6) and (7), the piston's natural frequencies are estimated to be about 70 Hz, 41 Hz and 33 Hz at the piston's positions X_0, X_1 and X_2, respectively. Further improvements to the mathematical model and the input data would be needed to achieve a better absolute agreement with the experimental results.

The frequency component of 119 Hz, which was observed only in the initial transient, probably represents some higher harmonic frequency of the piston oscillator. There were some speculations that it could be linked to the natural frequency of the fluid oscillator, but additional tests showed that both frequencies of 39 Hz and 119 Hz remain nearly the same for a connecting tube of twice the length. If dealing with the fluid oscillator, the natural frequency would vary approximately in inverse proportion to the square root of the length of the connecting tube, see, e.g., [13, 14].

4.2. Pressure response during the timing cycle of the piston stroke

In figure 5, the oscillating components of the pressure response are compared for two different flow rates during the timing cycle of the piston stroke. The pressure oscillations at the higher flow rate show a higher amplitude. The influence of the measured flow rate on the amplitude of the oscillations is presented in figure 6, which reports the computed experimental standard deviation of the pressure response during the timing cycle for different flow rates in the range from 1 sL min^{-1} to 45 sL min^{-1}. At least three measurements were performed at each flow rate. The amplitudes of the oscillations increase noticeably above flow rates of about 3 sL min^{-1} to 4 sL min^{-1}, with the largest values of the experimental standard deviation exceeding 50 Pa between 7.5 sL min^{-1} and 12.5 sL min^{-1}. To identify the pressure oscillations related only to the piston's motion, figure 6 also shows the experimental standard deviation of the pressure response for the bypass flow conditions, when the piston prover is not active. It is evident that the amplitudes of the pressure oscillations for the bypass flow are lower than those during the timing cycle in the entire flow range investigated; however, the relative differences between them decrease at higher flow rates.

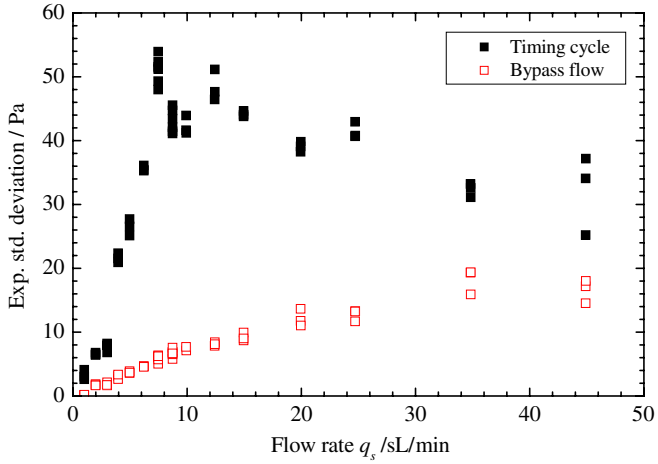

Figure 6. Experimental standard deviation of the measured pressure response during the Δt period and for the bypass flow conditions.

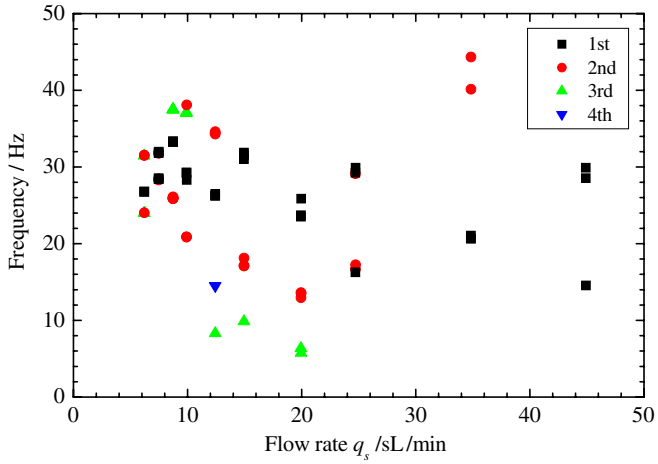

Figure 7. The largest frequency components of the measured pressure response during the Δt period.

A further analysis of the pressure pulsations during the measurement piston stroke was performed using a Fourier frequency analysis. A LabVIEW routine 'Extract Multiple Tone Information' was employed in the calculations. Figure 7 shows all the resulting frequency components that have RMS amplitudes higher than 15 Pa. They are sorted in descending order in terms of the amplitudes, from 1st to 4th (the number of frequency components with RMS amplitudes higher than 15 Pa is a maximum of four). The largest frequency components ('1st' data set in the graph) are all found between 15 Hz and 35 Hz. Taking into account the range of the natural frequencies of the piston oscillator estimated in section 4.1 (see figure 4), the observed dynamic responses could be reasonably related to the resonance effects of the piston oscillator.

An interesting insight into the dynamic processes within the piston prover is given in figure 8, where the frequencies from figure 7 are normalized with the flow rate. The frequencies of the pressure signals are found not to be random. They lie at characteristic levels, where the ratio between the frequency and the flow rate is constant (these levels are marked with dashed lines in figure 8). This means that all the frequencies at a particular level vary approximately linearly

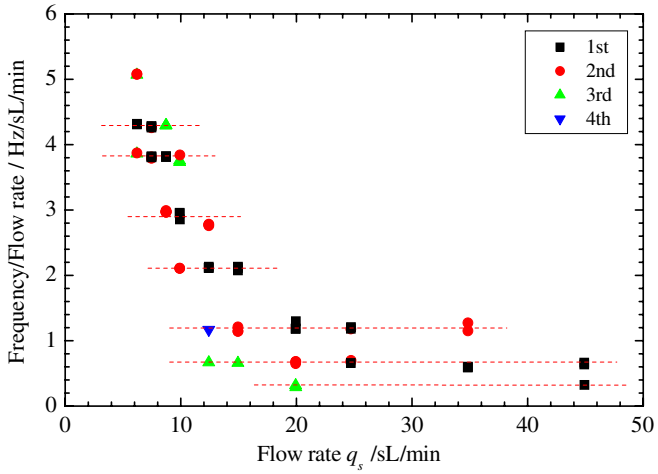

Figure 8. Normalized largest frequency components of the measured pressure response during the Δt period.

with the flow rate. Such results show that the origin of the piston's resonance is not stochastic, but is probably driven by a mechanism for which the characteristic frequencies are approximately proportional to the flow rate.

Such an excitation mechanism could be related to the effects of the inlet flow conditions in the cylinder below the moving piston. In the piston prover under discussion, the inlet port has an internal diameter of about 15 mm, which means it is about three times smaller than the cylinder diameter, and is positioned at the centre, at the bottom of the cylinder. There is also a temperature sensor with a diameter of about 1 mm to 2 mm, positioned transversely to the gas flow in the inlet port. (The given dimensions of the inlet port and the temperature sensor were approximately estimated from the outside through the transparent cylinder walls.) Such a configuration can undergo different self-sustained flow oscillations, which have characteristic frequencies linearly dependent on the flow rate. For instance, the flow over the temperature sensor could result in periodic vortex shedding [15, 16]. The flow from the inlet port into the gas cavity below the piston could be interpreted as a confined/impinging jet flow, which can turn into a periodically unstable flow as a result of different feedback mechanisms [16–18]. The interaction of both phenomena is also possible; see, e.g., [19, 20]. Each level of the frequency-to-flow-rate ratio in figure 8 can be interpreted as a different mode/harmonic of the flow instabilities.

Periodic flow instabilities below the piston probably result in a periodic fluid loading on the piston. Taking into account the asymmetric nature of the discussed flow instabilities, a rocking motion of the piston may also be induced. The gas clearance between the piston and the cylinder is about 10 µm in the device under discussion [7]. Therefore, even piston rocking of the order of a few micrometres may modify the sideways forces on the piston (such as the viscous drag force), which depend on the form of the gas clearance. Excessive rocking oscillations may also lead to the piston knocking against the cylinder walls.

As an illustration, figure 9 shows the resonant effect in the piston prover simulated by the mathematical model in

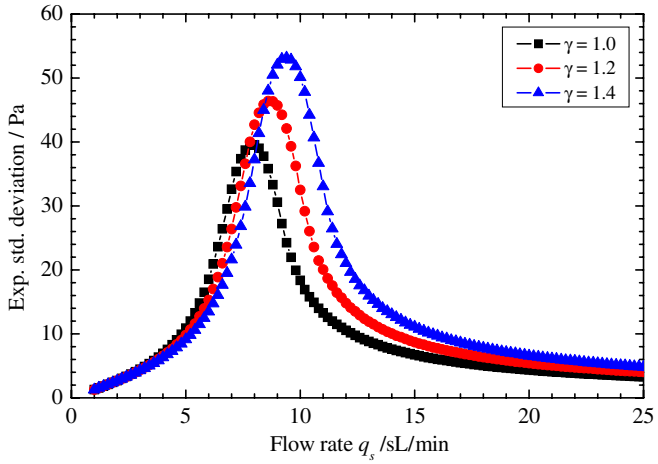

Figure 9. Experimental standard deviation of the pressure response during the Δt period for three different values of γ (simulation).

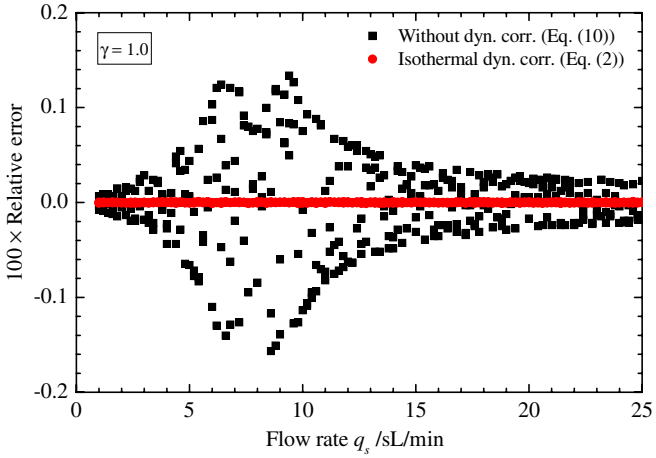

Figure 10. Relative error of the flow rate with and without a dynamic pressure correction for $\gamma = 1$ (simulation).

section 2. The excitation was introduced through a single-frequency sinusoidal time variation of the damping constant c in equation (3), with the frequency f_c changing linearly with the flow rate:

$$c \to c\,[1 + \varepsilon_c \sin(2\pi f_c t + \phi_c)]\,, \tag{9}$$

where $f_c = q_s f_{c0}/q_{s0}$ with $f_{c0} = 40$ Hz at $q_{s0} = 10\,\mathrm{sL\,min^{-1}}$, $\varepsilon_c = 0.25$ is the relative amplitude of the damping constant's oscillations and ϕ_c is the random initial phase uniformly distributed over the interval $[-\pi, \pi]$. Simulations were carried out for three values of the polytropic index γ from 1 to 1.4. The higher value of γ causes a shift of the resonant peak to higher flow rates due to the higher natural frequencies of the piston oscillator; see equation (8). It is evident that the pressure pulsations are amplified when the excitation frequency falls in the region of the natural frequencies of the piston oscillator.

5. Correction of dynamic effects due to pressure variations

In this section we use the above simulation example of the resonant effect (figure 9) for an evaluation of the flow measurements by the piston prover under dynamic conditions. We observe the relative errors of the estimated flow rate by the piston prover for three variants of the flow equations:

(i) flow equation without dynamic correction (10), which simulates the case when the slow-response pressure sensor measures only the steady-state pressure ($p_1 = p_2 = P$):

$$q_s^{(0)} = \frac{V_m}{\Delta t}\frac{P}{p_s}\frac{T_s}{T} + q_{s,l}, \tag{10}$$

(ii) isothermal flow equation (2), which is employed in the clearance-sealed piston prover used in the experimental work of this paper,

(iii) polytropic flow equation (12), which is derived by the authors of this paper in the continuation of this section.

The relative flow rate error was calculated as the relative deviation between the flow rate estimated by the selected flow

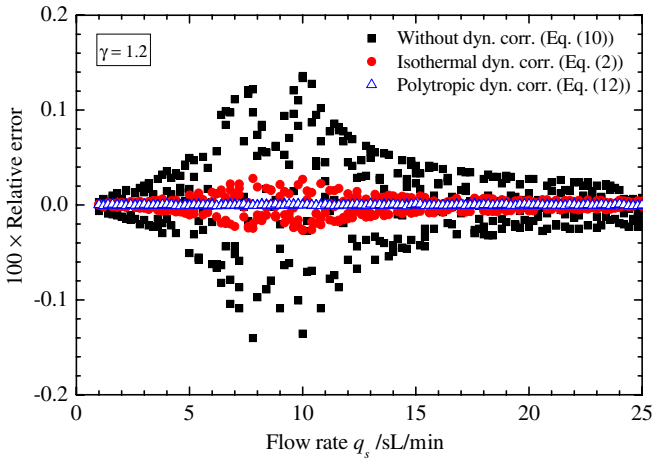

Figure 11. Relative error of the flow rate with and without a dynamic pressure correction for $\gamma = 1.2$ (simulation).

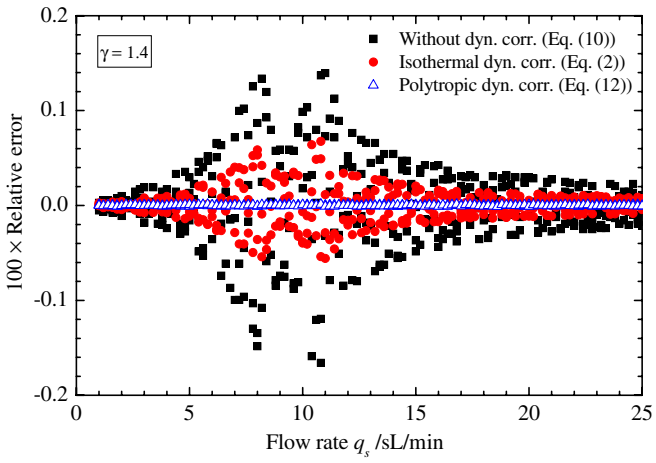

Figure 12. Relative error of the flow rate with and without a dynamic pressure correction for $\gamma = 1.4$ (simulation).

equation and the actual inlet flow rate defined as the input of the mathematical model.

Figures 10, 11 and 12 show the variation of the relative errors with the flow rate for three values of the polytropic

index γ of 1, 1.2 and 1.4, respectively. The use of the flow equation without a dynamic correction (10) leads to flow rate errors of up to 0.15% for all the simulated cases. The errors have two peaks in the range of the resonance effects in the piston prover. The resonance in these simulations occurs when the damping force, the frequency of which increases linearly with the flow rate, excites the piston at the natural frequency. The two error peaks are related to the resonance at the piston positions X_1 and X_2, which results in the amplified amplitudes of the pressure oscillations p_1 and p_2, respectively. As discussed in section 4, the piston's natural frequency becomes smaller at the piston position X_2 than at the piston position X_1. Therefore, the error peak at the smaller flow rate (with the smaller excitation frequency) corresponds to the maxima of the pressure oscillations at X_2, but the error peak at the higher flow rate (with higher excitation frequency) corresponds to the maxima of the pressure oscillations at X_1.

If the flow rate is calculated using the isothermal flow equation (2), including the estimated dynamic pressures at the times t_1 and t_2, the relative errors become practically zero for the isothermal simulation case $\gamma = 1$, which is shown in figure 10 (the very small remaining errors result from the effects of the time resolution of the simulations). However, fast processes with respect to heat exchange can often be considered as adiabatic or polytropic. The simulation results for $\gamma = 1.2$ and $\gamma = 1.4$ (figures 11 and 12) show some deficiency of equation (2), when it is employed to correct for the adiabatic or polytropic pressure oscillations. The remaining errors of the flow rate increase with the polytropic index γ.

The cause can be the fact that the gas temperature is not constant in the adiabatic or polytropic processes. Because the accurate temperature sensing of high-frequency temperature oscillations (of the same frequency as the pressure oscillations) can be difficult to realize in the piston prover, we tried to find a better relation between the gas density and the adiabatic or polytropic pressure oscillations. The relationship valid for a closed thermodynamic system is $p/\rho^{\gamma} = \text{const}$ [13]. Assuming small pressure variations p' with respect to a steady-state pressure P, the gas density can be approximated as

$$\rho = \bar{\rho} + \rho' = \bar{\rho}\left(1 + \frac{p'}{\gamma P}\right), \tag{11}$$

where $\bar{\rho} = P/(RT)$ represents a steady-state value. We employed equation (11) to define the modified flow equation of the piston prover:

$$q_s = \frac{V_m}{\Delta t}\left(\frac{P + p_2'/\gamma}{p_s} + \frac{p_2'/\gamma - p_1'/\gamma}{p_s}\frac{V_d}{V_m}\right)\frac{T_s}{T} + q_{s,1}. \tag{12}$$

or

$$q_s = q_s^{(0)}\left\{1 + \frac{1}{\gamma}\left[\left(1 + \frac{V_d}{V_m}\right)\frac{p_2'}{P} - \frac{V_d}{V_m}\frac{p_1'}{P}\right]\right\}. \tag{13}$$

The polytropic conditions show the dynamic effect on the measured flow rate, which is a factor γ smaller than that in the isothermal system. The simulation results for $\gamma = 1.2$ and $\gamma = 1.4$ (figures 11 and 12) demonstrate the successful correction of the dynamic effects if the proposed flow equation (12) is applied to estimate the flow rate.

Using the polytropic flow equation (12) in the piston prover would demand the estimation of the effective polytropic index γ, which suits the thermodynamic nature of the gas processes in the piston prover. For random dynamic effects, it could be estimated experimentally by looking for a minimum of the experimental standard deviation of repeated measurements at a constant inlet flow rate.

In general, the processes during the piston prover's operation can also involve relatively slow variations of the gas density, which for example result from temperature variations due to the heat transfer over the system boundaries, changes in the atmospheric pressure, etc. It would be correct to separate these variations from fast polytropic, or adiabatic, oscillations. Starting from the general flow equation of the piston prover (1), the modified expression for gas density (11) can be employed separately for $\rho_{d,1}$, $\rho_{d,2}$ and $\rho_{m,2}$, where $\bar{\rho}_{d,1}$, $\bar{\rho}_{d,2}$ and $\bar{\rho}_{m,2}$ are determined from the low-pass filtered values of pressures and temperature, and $\rho'_{d,1}$, $\rho'_{d,2}$ and $\rho'_{m,2}$ from the corresponding pressure oscillations and estimated polytropic index.

6. Comments on the repeatability of the piston prover

The repeatability of the clearance-sealed piston prover under discussion was experimentally estimated by ten consecutive flow readings at different flow rates in its measuring range. The largest relative deviations from the average value were up to 0.04% at gas flow rates below 20 sL min^{-1}, but reached values of 0.08% at higher flow rates. On the basis of the findings presented in the previous sections it can be concluded that the pressure correction carried out in the piston prover seems to be at least partially successful. For example, considering the amplitudes of the measured pressure oscillations at flow rates up to 20 sL min^{-1} in section 4 and the estimated flow errors without the dynamic pressure correction in section 5, a relative scatter of measured values exceeding 0.1% would be expected without dynamic corrections.

In the interpretation of the above-estimated random variations we have to consider that it is hard to distinguish the potential, non-ideally corrected, dynamic influences related to the gas density from other contributions. In addition to the dynamic influences, there are other random effects, such as the quantization and repeatability/reproducibility of the measurement equipment used (measuring the time, the pressure, the temperature) [6]. Smaller time differences could be one of the reasons for the greater relative scatter at higher flow rates. The second possibility is the uncorrected dynamical influences, e.g. the effects of high-frequency pressure pulsations, which are not spatially homogeneous over the entire volume, piston rocking and so on. Piston rocking, which in section 4.2 was described as having a potential contribution to the pressure oscillations, also represents an error source for the cylinder volume or the time measurement. In [5] the error of the cylinder volume due to piston rocking was eliminated by employing a laser interferometer, which has a laser reflector installed on the centre of the piston's top surface.

The second question that arises is as follows: to what extent are the dynamic effects actually random and to what extent are they systematic? The simulation results in section 5 show a certain degree of random scatter, which is the consequence of the assumed random initial phase of the added disturbance in equation (9). However, if the source of the excitation mechanism is linked to the piston stroke's sequence, the resulting dynamic pressure conditions could have a deterministic nature and therefore could be repeated during the next measurement performed under the same conditions. Such qualitatively repeatable variations of the pressure amplitudes are evident in figure 2(*b*). In such a case it is possible that the uncorrected dynamic effects would not only reflect the deteriorated repeatability of the flow meter, but also its systematic error.

7. Conclusions

The investigation presented in this paper consists of two main parts. In the first part we analysed the dynamic pressure responses that were measured during the operation of the clearance-sealed realization of the piston prover. And in the second part, we dealt with an estimation of the effects of such dynamic pressure conditions on the measured flow rate by the piston prover. Both the experimental methods and the lumped-element mathematical modelling were combined in the research work. Here, we summarize some of the most important findings:

- The measurements in the initial phase of the piston stroke detect damped pressure oscillations, which result from the switching of the bypass valve and redirecting the flow into the measuring cylinder. Considering the relatively short duration of the pressure transient, no significant influence of such a transient pressure response is expected in the timing cycle of the discussed realization of the piston prover. One of the identified frequencies in the initial transient can be related to the natural frequency of the piston mass on the gas spring (the piston oscillator). This natural frequency decreases during the piston motion due to the increased gas volume.
- The pressure oscillations that were measured during the timing cycle show a significant increase in amplitude above a certain flow rate and multiple frequency components. The frequencies of all the highest components lie at characteristic levels, where the ratio between the frequency and the flow rate is constant. This means that all the frequencies at a particular level vary approximately linearly with the flow rate. Such a pressure response could be related to the resonance effects of the piston oscillator, which are excited by the self-sustained oscillations of the inlet flow in the cylinder below the moving piston (periodic jet and wake flow instabilities).
- The simulation results have shown that the thermodynamic nature of gas processes, which occur in piston provers under dynamic conditions, should be taken into account for the successful correction of dynamic errors. If the dynamic processes could be assumed to be isothermal, it is sufficient to consider the dynamic pressures at the start and at the end of the timing cycle. On the other hand, if the dynamic processes are adiabatic or polytropic, the temperature also becomes an important variable. We derived a new, modified flow equation of the piston prover, where non-isothermal conditions are taken into account by the effective value of the polytropic index. The validation of the proposed polytropic correction model using theoretical simulations was successful.

In spite of many new findings about the effects of dynamic pressure on the measurement accuracy and the operation of piston provers in this paper, there are still open questions for further research in this field:

- In the scope of this paper we did not physically modify the compact design of the flow cell of the piston prover that was used in the experimental studies. If the identified resonance effects are really significantly related to the excitation mechanisms of the inlet flow instabilities, then a suitable design of that inlet part of the measurement device could reduce the observed dynamic phenomena.
- The identified flow-induced vibrations in the system with a moving piston call for further phenomenological study. They could be, for instance, investigated experimentally by local measurements of the flow parameters in the cylinder or numerically by a three-dimensional coupled fluid–solid model. The research of such a physical system is, in addition to the piston provers for flow rate measurements, also relevant for pneumatic cylinders, Stirling engines and so on.
- The validation of the proposed polytropic model for the correction of dynamic pressure conditions remained at the level of the lumped-element dynamic model in this paper. The modified model was not implemented in the observed commercial design of the piston prover, because it is not trivial for a user to alter its computational algorithms. A further systematic experimental analysis has to be performed to confirm its applicability.

References

[1] Wright J D and Mattingly G E 1998 *NIST Calibration Services for Gas Flow Meters—Piston Prover and Bell Prover Gas Flow Facilities* National Institute of Standards and Technology

[2] Wright J D, Mattingly G E, Nakao S, Yokoi Y and Takamoto M 1998 International comparison of a NIST primary standard with an NRLM transfer standard for small mass flow rates of nitrogen gas *Metrologia* **35** 211–21

[3] Berg R F and Cignolo G 2003 NIST–IMGC comparison of gas flows below one litre per minute *Metrologia* **40** 154–8

[4] Cignolo G, Alasia F, Capelli A, Goria R and La Piana G 2005 A primary standard piston prover for measurement of very small gas flows: an update *Sensor Rev.* **25** 40–5

[5] Choi H M, Park K-A, Oh Y K and Choi Y M 2009 Improvement and uncertainty evaluation of mercury sealed piston prover using laser interferometer *Flow Meas. Instrum.* **20** 200–5

[6] Padden H 2002 Uncertainty analysis of a high-speed dry piston flow prover *Measurement Science Conf. (Anaheim, CA)*

[7] Padden H 2003 Development of a 0.2% high-speed dry piston prover *Measurement Science Conf. (Anaheim, CA)*
[8] Padden H 2004 Dynamic error correcting positive displacement piston flowmeter and method of measuring gas flow in a piston flowmeter *US Patent* 6763731 B1
[9] Wu J, Goldfarb M and Barth E 2004 On the observability of pressure in a pneumatic servo actuator *J. Dyn. Syst. Meas. Control* **126** 921–4
[10] Dihovicni D and Nedić N 2008 Simulation, animation and program support for a high performance pneumatic force actuator system *Math. Comput. Modelling* **48** 761–8
[11] Parlak N, Wagner A, Elsner M and Soyhan H S 2009 Thermodynamic analysis of a gamma type Stirling engine in non-ideal adiabatic conditions *Renew. Energy* **34** 266–73
[12] Waele A T A M 2009 Basic treatment of onset conditions and transient effects in thermoacoustic Stirling engines *J. Sound Vibration* **325** 974–88
[13] Blevins R D 1995 *Formulas for Natural Frequency and Mode Shape* (Malabar, FL: Krieger)
[14] Bajsić I, Kutin J and Žagar T 2007 Response time of a pressure measurement system with a connecting tube *Instrum. Sci. Technol.* **35** 399–409
[15] Blevins R D 1994 *Flow-Induced Vibration* (Malabar, FL: Krieger)
[16] Nausdacher E and Rockwell D 1994 *Flow-Induced Vibrations: An Engineering Guide* (Rotterdam: Balkema)
[17] Maurel A, Ern P, Zielinska B J A and Westfried J E 1996 Experimental study of self-sustained oscillations in a confined jet *Phys. Rev.* E **54** 3643–51
[18] Shakouchi T, Suematsu Y and Ito T 1982 A study on oscillatory jet in cavity (first report, Mechanism of Oscillation) *Bull. JSME* **25** 1258–65
[19] Chou Y W, Hsiao F B, Hsu C C and Huang J M 2002 Vortex dynamics and energy transport of a plane jet impinging upon a small cylinder *Exp. Thermal Fluid Sci.* **26** 445–54
[20] Hsiao F B, Hsu I C and Huang J M 2004 Evolution of coherent structures and feedback mechanism of the plane jet impinging on a small cylinder *J. Sound Vibration* **278** 1163–79